
FouriDown: Factoring Down-Sampling into Shuffling and Superposing

Qi Zhu ^{1,*}, Man Zhou ^{2,3,*}, Jie Huang ¹, Naishan Zheng ¹, Hongzhi Gao ¹,
Chongyi Li ⁴, Yuan Xv ³, Feng Zhao ^{1†}

¹University of Science and Technology of China,

²S-Lab, ³Nanyang Technological University, ⁴Nankai University

{zqcrafts, hj0117, nszheng, hongzhigao}@mail.ustc.edu.cn,

{man.zhou, xu.yuan}@ntu.edu.sg, lichongyi25@gmail.com, fzhao956@ustc.edu.cn

Abstract

Spatial down-sampling techniques, such as strided convolution, Gaussian, and Nearest down-sampling, are essential in deep neural networks. In this paper, we revisit the working mechanism of the spatial down-sampling family and analyze the biased effects caused by the static weighting strategy employed in previous approaches. To overcome the bias limitation, we propose a novel down-sampling paradigm in the Fourier domain, abbreviated as FouriDown, which unifies existing down-sampling techniques. Drawing inspiration from the signal sampling theorem, we parameterize the non-parameter static weighting down-sampling operator as a learnable and context-adaptive operator within a unified Fourier function. Specifically, we organize the corresponding frequency positions of the 2D plane in a physically-closed manner within a single channel dimension. We then perform point-wise channel shuffling based on an indicator that determines whether a channel’s signal frequency bin is susceptible to aliasing, ensuring the consistency of the weighting parameter learning. FouriDown, as a general operator, comprises four key components: 2D discrete Fourier transform, context shuffling rules, Fourier weighting-adaptively superposing rules, and 2D inverse Fourier transform. These components can be easily integrated into existing image restoration networks. To demonstrate the efficacy of FouriDown, we conduct extensive experiments on image de-blurring and low-light image enhancement. The results consistently show that FouriDown can provide significant performance improvements. The code is publicly available to facilitate further exploration and application of FouriDown at <https://github.com/zqcrafts/FouriDown>.

1 Introduction

Down-sampling technique [1, 2, 3] plays a vital role in deep neural networks because of its benefits in enlarging the receptive field, extracting hierarchical features, improving computational efficiency, and handling scale and translation variations. However, based on the signal sampling theorem, existing down-sampling techniques such as strided convolution, Gaussian, and Nearest down-sampling [1, 4, 5, 6] unavoidably reduce the sampling frequency of discrete signals, leading to unexpected frequency aliasing where high frequencies are folded into low frequencies.

To address the aliasing problem, several strategies [7, 8, 9, 10, 11, 12, 13] have been developed. They pre-process the signals applying the low-pass filtering mechanism, which aims to filter out high-frequency information by employing different types of low-pass designs. There are two commonly

*Both authors contributed equally to this research.

†Corresponding author.

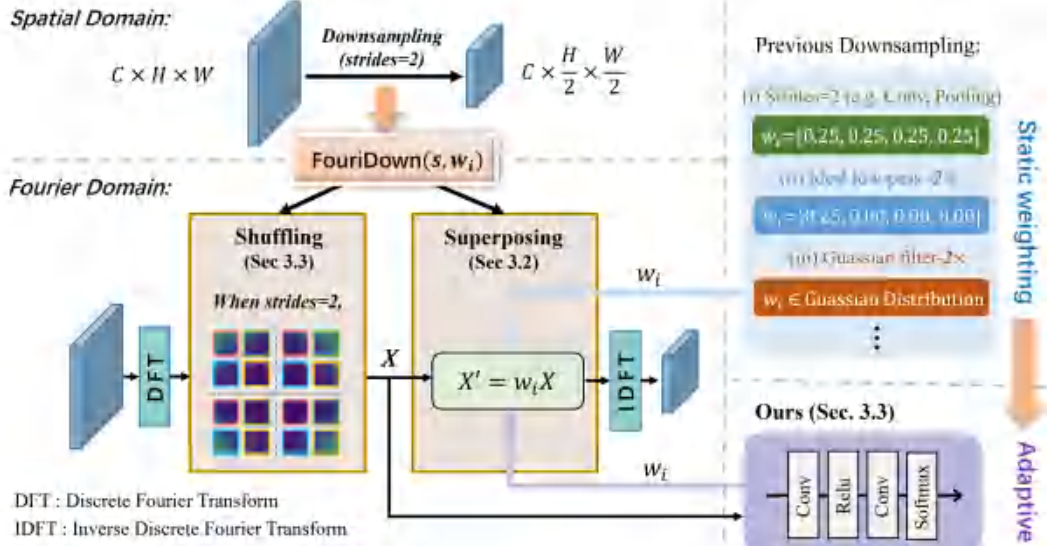


Figure 1: Comparison on the flowcharts of different down-sampling techniques in $2 \times$ scale. The previous spatial down-sampling community stands on the static weighting templates and is not relevant with the image context. By contrast, inspired by the signal sampling theorem, we parameterize the static weighting down-sampling operator as a learnable and context-adaptive operator in a unified Fourier function.

used types including the ideal low-pass filter that truncates high frequencies in the Fourier domain and the Gaussian low-pass filter that gradually attenuates frequency components near the boundary. However, the ideal low-pass filter may introduce ring artifacts due to spectrum leakage, while the Gaussian low-pass filter may result in a significant loss of edge information that is crucial for visual recognition tasks.

The prevailing approaches in the down-sampling family rely on a static weighting strategy, which may lead to unintended biases (See Section 4.4 for details.). As described in Figure 1, strided convolution and strided pooling variants rely on the static template $w_i = [0.25, 0.25, 0.25, 0.25]$ over the corresponding cornered positions while the ideal low-pass one exploits the $w_i = [0.25, 0, 0, 0]$ weighting template. (See Appendix B for proofs.) All of them are shared over all the coordinated positions and uninvolved with the feature context. It is widely acknowledged that the static sampling approach, which lacks contextual relevance, is sub-optimal for visual tasks. Therefore, both bridging different down-sampling approaches and achieving an optimal approach are desirable, as shown in Figure 1 where we focus on unifying the down-sampling modeling rules in a learnable and context-adaptive parameterized function in Fourier domain.

In this study, we delve into the working mechanism of the spatial down-sampling family and analyze the biased effects resulting from the static weighting strategy used in existing down-sampling approaches. To solve the bias problem, we propose a novel down-sampling paradigm called FouriDown, which operates in the Fourier domain and adapts the feature sampling based on the image context. Inspired by the signal sampling theorem, we parameterize the non-parameter static weighting down-sampling operator as a learnable and context-adaptive operator in a unified Fourier function. Furthermore, drawing from this insight, we organize the corresponding frequency positions of the 2D plane, ensuring that they are physically closed in a single channel dimension. We then perform point-wise channel shuffling based on an indicator that determines whether a channel’s signal frequency bin is prone to aliasing, thereby maintaining the consistency of the weighting parameter learning. FouriDown, as a generic operator, comprises four key components: 2D discrete Fourier transform, context shuffling rules, Fourier weighting-adaptively superposing rules, and 2D inverse Fourier transform. These components can be readily integrated into existing image restoration networks, allowing for a plug-and-play approach. To verify its efficacy, we conduct extensive experiments across multiple computer vision tasks, including image de-blurring and low-light image enhancement. The results demonstrate that FouriDown consistently outperforms the baselines, showcasing its capability of performance improvement.

In conclusion, this work propose a novel and unified framework for the research of down-sampling, which have the following contributions.

- 1) We provide the first exploration of the aliasing problem in deep neural networks, analyzing it from a spectrum perspective.
- 2) To achieve dynamic frequency aliasing, we introduce a unified approach to down-sampling strategies within the Fourier function. Additionally, we propose a learnable and context-adaptive down-sampling operator based on the Nyquist signal sampling theorem.
- 3) Our proposed down-sampling approach serves as a plug-and-play operator, consistently enhancing the performance of image restoration tasks, such as low-light enhancement and image deblurring.

2 Related Work

2.1 Traditional Down-Sampling

Downsampling is an important and common operator in computer vision [14, 15, 16, 17, 18, 19, 20, 21, 22, 23, 24, 25], which benefits from enlarging the receptive field and reducing computational costs. So many models incorporate downsampling to allow the primary reconstruction components conducting at a lower resolution. Moreover, with the emergence of increasingly compute-intensive large models, downsampling becomes especially crucial, particularly for high-resolution input images.

Previous downsampling methods often utilized local spatial neighborhood computations (e.g., Bilinear, Bicubic and MaxPooling), which show decent performances across various tasks. However, these computations are relatively fixed, making it challenging to maintain consistent performance across different tasks. To address this, some methods made specific designs to make the downsampling more efficient in specific tasks. For instance, some works [12, 11, 10, 7] introduce the Gaussian blur kernel before the downsampling convolution to combat aliasing for better shift-invariance in classification tasks. Grabinski et al. [26, 27] equip the ideal low-pass filter or the hamming filter into downsampling to enhance model robustness and avoid overfitting.

2.2 Dynamic Down-Sampling

Due to the development of data-driven deep learning, in addition to traditional down-sampling, some other works [28, 29, 30, 31, 32, 33] introduce dynamic downsampling to adaptively adjust for different tasks, thereby achieving better generalizability. For instance, Pixel-Shuffle [28] enables dynamic spatial neighborhood computation through the interaction between feature channels and spaces, restoring finer details more effectively. Kim et al. [29] proposes a task-aware image downsampling to support upsampling for more efficient restoration.

In addition to dynamic neighborhood computation, dynamic strides have also gained widespread attention in recent years. For instance, Riad et al. [30] posits that the commonly adopted integer stride of 2 for downsampling might not be optimal. Consequently, they introduce learnable strides to explore a better trade-off between computation costs and performances. However, the stride is still spatially uniformly distributed, which might not be the best fit for images with uneven texture density distributions. To address this issue, dynamic non-uniform sampling garners significant attention [31, 32, 33]. For example, Thavamani et al. [31] proposed a saliency-guided non-uniform sampling method aimed at reducing computation while retaining task-relevant image information.

In conclusion, most of recent researches focus on dynamic neighborhood computation or dynamic stride for down-sampling, where the paradigm can be represented as $Down(s)$, where s denotes the stride. However, in this work, we observe that the methods based on this downsampling paradigm employ static frequency aliasing, which may potentially hinder further development towards effective downsampling. However, learning dynamic frequency aliasing upon the existing paradigm poses challenges. To address this issue, we revisit downsampling from a spectral perspective and propose a novel paradigm for it, denoted as $FouriDown(s, w)$. This paradigm, while retaining the stride parameter, introduces a new parameter, w , which represents the weight of frequency aliasing during downsampling and is related to strides. Further, based on this framework, we present an elegant and effective approach to achieve downsampling with dynamic frequency aliasing, demonstrating notable performance improvements across multiple tasks and network architectures.

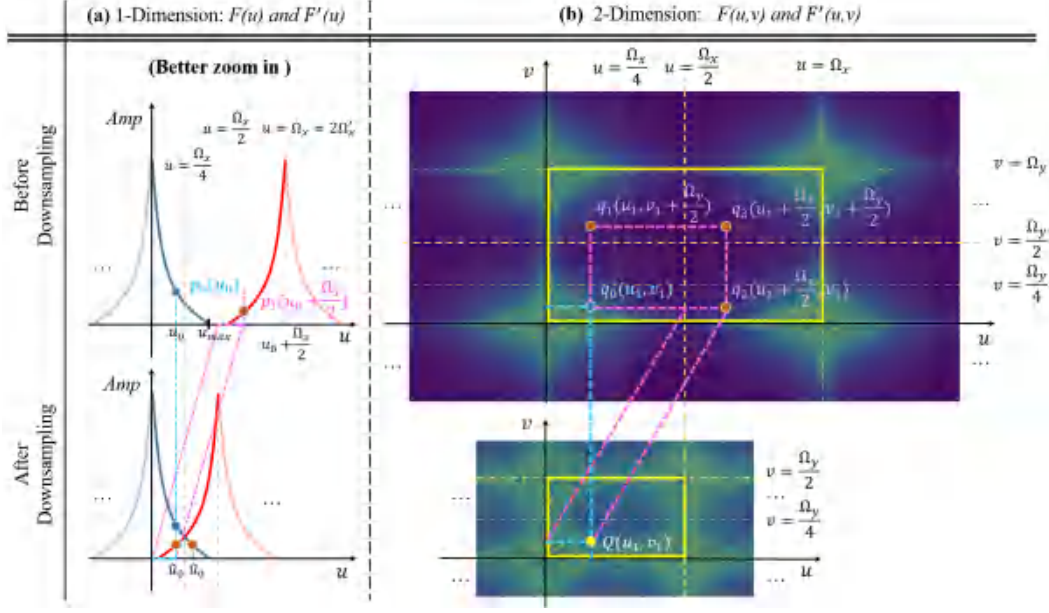


Figure 2: The visualization of the shuffling and superposing theory in the 1-D and 2-D signals.

3 Method

Definitions. $f(x, y) \in \mathbb{R}^{H \times W \times C}$ is the 2-D discrete spatial signal and the sampling rates in x and y axis are Ω_x and Ω_y , respectively. $F(u, v) \in \mathbb{R}^{H \times W \times C}$ is the Fourier transform of $f(x, y)$, where the maximum frequencies in u and v axis are respectively denoted as u_{max} and v_{max} . Moreover, $f'(x, y) \in \mathbb{R}^{\frac{H}{2} \times \frac{W}{2} \times C}$ is 2-strided down-sampled $f(x, y)$ and its Fourier transform $F'(u, v)$.

Theorem-1. Shuffling and Superposing. The spatial down-sampling typically results in a shrinkage of the tolerance for the maximum frequency of the signal. Specifically, high frequencies will fold back into new low frequencies and superpose onto the original low frequencies. To illustrate with 1-dimensional signal, the high and low frequency superposition in the down-sampling can be formulated as

$$F'(u) = \mathbb{S}(F(u), F(u + \frac{\Omega_x}{2})) \quad \text{when } u \in (0, \frac{\Omega_x}{2}), \quad (1)$$

where \mathbb{S} is a superposing operator. Note that the high frequency is $F(u + \frac{\Omega_x}{2})$ considering positive directions, while the low frequency is $F(u)$ considering positive directions instead.

Theorem-2. Static Averaging Superposing. For an image, the spatial down-sampling operator with 2 strides can be equivalent to dividing the Fourier spectrum into 2×2 equal parts and superposing them averagely by $\frac{1}{4}$ factor

$$F(u, v) = \left[\begin{array}{c} F_{(0,0)}(u, v) + F_{(0,1)}(u, v) \\ F_{(1,0)}(u, v) + F_{(1,1)}(u, v) \end{array} \right], \quad (2)$$

where $F_{(i,j)}(u, v)$ is a sub-matrix of $F(u, v)$ by equally dividing $F(u, v)$ into 2×2 partitions and $i, j \in \{0, 1\}$. Given that Down_2 is 2-strided down-sampling operator and IDFT is inverse discrete Fourier transform, we have

$$\text{Down}_2(f(x, y)) = \text{IDFT} \left(\frac{1}{4} \sum_{i=0}^1 \sum_{j=0}^1 F_{(i,j)}(u, v) \right). \quad (3)$$

The proof of the above theorem can be found in the Appendix, and examples of 1-D and 2-D signals can also be referred in Figure 2(a) and (b).

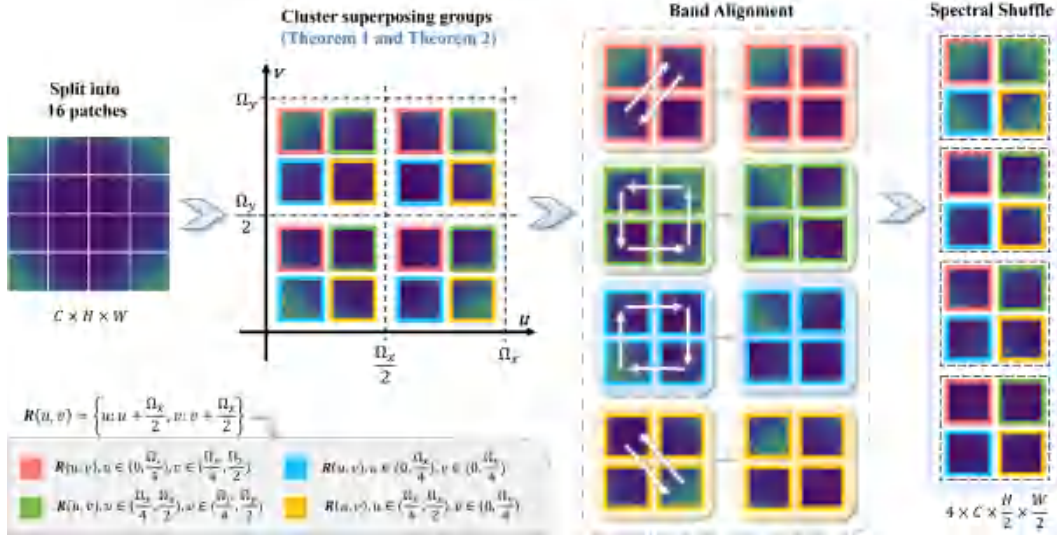


Figure 3: Overview of the proposed spectral shuffle.

Algorithm 1 Pseudo-code of FouriDown.

Data: Input: $x \in \mathbb{R}^{N \times C \times H \times W}$. Set of real numbers: \mathbb{R} . Set of complex numbers: \mathbb{C} .

Result: $y \in \mathbb{R}^{N \times C \times \frac{H}{2} \times \frac{W}{2}}$

```

 $x_{fft} \leftarrow FFT(x) \in \mathbb{C}^{N \times C \times H \times W}$  // Fast Fourier transform
 $x_{shuffle} \leftarrow Shuffle(x_{fft}) \in \mathbb{C}^{N \times 4 \times C \times \frac{H}{2} \times \frac{W}{2}}$ 
 $x_{weight} \leftarrow Softmax(Conv_{1 \times 1}(x_{shuffle}, groups = C)) \in \mathbb{C}^{N \times 4 \times C \times \frac{H}{2} \times \frac{W}{2}}$ 
 $x_{superposed} \leftarrow Sum(x_{weight} * x_{shuffle}, dim = 1) \in \mathbb{C}^{N \times C \times \frac{H}{2} \times \frac{W}{2}}$ 
 $y \leftarrow iFFT(x_{superposed})$  // Inverse Fourier transform

```

3.1 Architecture Design

In this work, we argue that the static superposing strategy like the stride-based down-sampling in Theorem-2 might lead to biased effects. Motivated by adaptively learning ability of CNNs, we aim to parameterize the non-parameter static superposing step as a learnable and context-adaptive operator in the Fourier domain.

Definition-2 (Shuffle-Invariance) Given an operator $z(\cdot)$ that is shuffle-invariant and o_1, o_2, o_3, o_4 as different components, the shuffle-invariant is defined as $z(o_1, o_2, o_3, o_4) = z(shuffle(o_1, o_2, o_3, o_4))$, where $shuffle(\cdot)$ is shuffling the order of input components arbitrarily.

Note that the average operator in Theorem-2 is shuffle-invariant. For example, $Aver(a, b, c, d) = Aver(b, a, c, d)$. However, different from averaging, the convolution operator, which is sensitive to the input order, does not have this property.

To alleviate this problem, we design a spectral-shuffle strategy that first performs shuffling according to Theorem-1 and then aligns across different frequency bands, as shown in Figure 3. Specifically, we initially split the original spectrum $F(u, v)$ into 16 patches equally. Then, according to Theorem-1, we classify these patches into 4 group, where each group is pixel-wise matched frequency bin for superposing. However, the energy distribution in each group is different. Considering the shuffle-variance of convolution operators, we reorder the intra-group sequence for inter-group alignment. The alignment is motivated by wavelet theory, where intra-group frequencies are reordered according to low-frequency and high-frequency in horizontal direction, high-frequency in vertical direction, and high-frequency in diagonal direction. Then, the aligned groups are sorted orderly on channels for pixel-wise matching in the channel dimension. Finally, we perform adaptively weighted superposition on channels by learned weights for the down-sampling results. The main implementation is depicted in Algorithm 1. Code will be public.

4 Experiments and Discussion

To validate the efficacy of our proposed FouriDown, we execute comprehensive experiments across several computer vision tasks and conduct exhaustive ablation studies to evaluate its resilience.

4.1 Experimental Settings

Image enhancement. For image enhancement, we assess our FouriDown model using the LOL [34] and Huawei [35] benchmarks. The LOL dataset contains 500 image pairs (485 for training, 15 for testing), and the Huawei dataset contains 2480 paired images (2200 for training, 280 for testing). We compare our results with two established baselines, SID [36] and DRBN [37].

Image deblurring. For image deblurring, we utilize DeepDeblur [38] and MPRNet [39] on the DVD dataset [40], which includes 2103 training and 1111 test pairs. We further validate our model’s generalizability using the HIDE dataset [41].

Image denoising. In the context of image de-noising, our training involves the SIDD dataset [42]. Subsequent performance assessments are carried out on the remaining validation samples from the SIDD dataset and on the DND benchmark dataset [43]. For comparative analysis, we choose baselines such as MIRNet [44], and Restormer [45].

Image dehazing. For image dehazing, we employ RESIDE dataset for evaluations. We also use two different network designs MSBDN [46] and GridNet [47] with our proposed operator for validation.

4.2 Implementation Details

Regarding the above competitive baselines, we perform the comparison over the following configurations by replacing the down-sampling operator, such as strided convolution and strided pooling), with the proposed FouriDown operator. Additionally, we also perform comparisons with previous anti-aliasing down-sampling methods, including Gaussian filter [7] and “ideal” Low-Pass Filter (LPF) [13], which conduct the static modulation on the spectrum.

- 1) **Original:** The original down-sampling in the baseline;
- 2) **Gaussian:** Following [7], equipping the Gaussian filter in all channels before the original down-sampling for anti-aliasing;
- 3) **LPF:** Following [13], equipping the “ideal” Low-Pass Filter in all channels before the original down-sampling operator for anti-aliasing;
- 4) **Ours:** Replacing our proposed FouriDown with the original down-sampling operator;

Table 1: Image enhancement comparison.

Method	Config	LOL		Huawei	
		PSNR	SSIM	PSNR	SSIM
DRBN	Original	19.92	0.7712	20.21	0.6742
	Gaussian	20.21	0.8146	20.66	0.6955
	LPF	18.91	0.7441	20.34	0.6812
	Ours	21.64	0.8513	21.46	0.7213
SID	Original	21.46	0.8584	20.38	0.6931
	Gaussian	21.78	0.8612	20.52	0.6926
	LPF	20.74	0.8124	20.54	0.6841
	Ours	23.28	0.8708	20.90	0.7002

Table 2: Image deblurring comparison.

Method	Config	DVD		HIDE	
		PSNR	SSIM	PSNR	SSIM
DeepDeblur	Original	29.32	0.8817	29.60	0.8849
	Gaussian	29.36	0.8823	29.62	0.8892
	LPF	29.19	0.8751	29.51	0.8851
	Ours	29.44	0.8856	29.70	0.8904
MPRNet	Original	30.12	0.8958	30.04	0.8945
	Gaussian	30.23	0.8922	30.06	0.8966
	LPF	30.00	0.8918	29.95	0.8937
	Ours	30.31	0.8996	30.25	0.9102

Table 3: Image de-noising comparison.

Method	Config	SIDD		DND	
		PSNR	SSIM	PSNR	SSIM
Restormer	Original	39.41	0.9171	39.67	0.9173
	Gaussian	39.43	0.9169	39.69	0.9177
	LPF	39.35	0.9162	39.64	0.9167
	Ours	39.47	0.9174	39.73	0.9180
MIRNet	Original	39.52	0.9182	39.41	0.9146
	Gaussian	39.55	0.9184	39.45	0.9148
	LPF	39.49	0.9179	39.35	0.9141
	Ours	39.64	0.9186	39.56	0.9251

Table 4: Image dehazing comparison.

Method	Config	Indoor		Outdoor	
		PSNR	SSIM	PSNR	SSIM
MSBDN	Original	29.77	0.9591	28.88	0.9581
	Gaussian	30.09	0.9607	28.91	0.9583
	LPF	29.92	0.9598	29.03	0.9591
	Ours	30.19	0.9612	29.21	0.9604
GridNet	Original	30.16	0.9616	29.54	0.9605
	Gaussian	30.21	0.9617	29.62	0.9622
	LPF	30.18	0.9611	29.58	0.9615
	Ours	30.42	0.9654	29.71	0.9641



Figure 4: Visual comparison of SID on the LOL dataset. FouriDown enhances the global color perception ability of the original model, thereby improving the model’s performance without adding extra parameters or computational overhead.

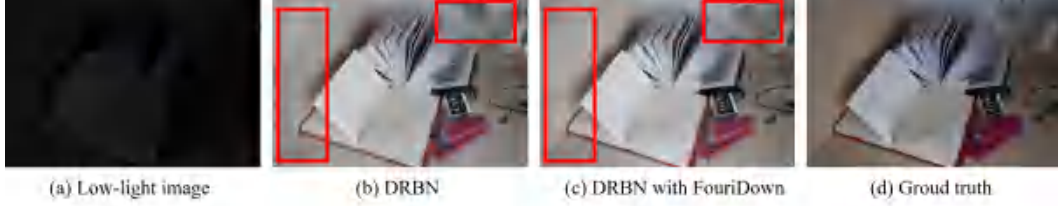


Figure 5: Visual comparison of DRBN on the LOL dataset. The more flexible frequency interaction mechanism in FouriDown reduces artifacts compared to the original methods.

4.3 Comparison and Analysis

Quantitative Comparison. To demonstrate the effectiveness of our proposed FouriDown, we conduct extensive experiments as shown in Tables 1-4. The best results are in bold. Above and below the baseline are highlighted in red and blue, respectively. From these tables, although previous anti-aliasing methods may be useful for some image restoration tasks, their static weights limit their universality in other tasks. For instance, while the LPF approach performs well in dehazing, it fails to deliver effective in deblurring and low-light enhancement. In contrast, our method is proved to be effective across the majority of image restoration tasks. Specifically, we achieved an improvement of 1.82dB in low-light enhancement and 0.42dB in dehazing on LOL and Reside dataset respectively.

Further, we compare the computing costs with other methods shown in Table 5. We include results from traditional down-sampling techniques like bicubic, bilinear, pixel-unshuffle, 2x2 learnable CNN (with stride=2), max-pooling, average-pooling, LPF, Gaussian and Ours. Noting that the “Original” down-sampling of the method is pointed by asterisk (*). This will allow a clearer contrast and showcase the advantages of our method not only against anti-aliasing approaches but also against these conventional down-sampling methods.

Qualitative Comparison. Due to space constraints, we only present a qualitative comparison on the low-light enhancement task. As illustrated in Figure 4 and Figure 5, our FouriDown reduces original artifacts presented in the SID due to the more flexible frequency interactions. Then, we compare the visualizations of the feature maps and their corresponding spectra between FouriDown and other down-sampling methods (see Figure 6 and Figure 7). It can be observed that the model equipped with FouriDown generates much stronger responses to degradation-aware regions, i.e. global low-illumination in the low-light enhancement task. In contrast, the model with other down-sampling method responds weakly to these regions. The results demonstrates the effectiveness of FouriDown in capturing degradation-aware information by adaptive frequency superposition in down-sampling. For the Gaussian method, its response to degradation is relatively large (second only to FouriDown), thus achieving performance that is also second only to FouriDown. Similarly, as the LFP method has the poorest performance, its feature response of the low-light areas is also the lowest. The performance of other methods is roughly similar, so their feature responses are also quite similar, indicating a similar capability to capture image degradation areas. Additionally, from the spectral comparison in Figure 7, it can be observed that the Gaussian method loses a lot of high-frequency information compared to FouriDown. This leads to challenges in recovering textures in dark areas. Hence, although the Gaussian method exhibits good responses, FouriDown achieves better performances compared to it. More qualitative comparisons can be found in the following supplementary material.



Figure 6: Feature comparison between our FouriDown and other down-sampling methods in low-light enhancement task. Due to the unique global modeling mechanism in the frequency domain, the features extracted by our method significantly achieve a larger response than others.

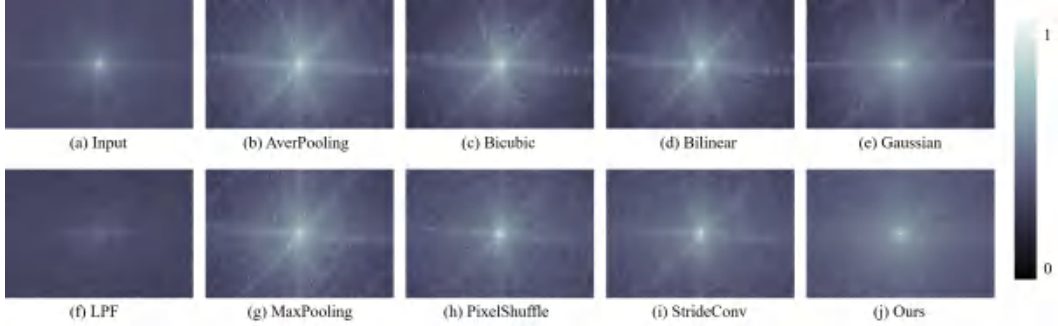


Figure 7: Spectrum comparison of the feature maps in Figure 6. The spectrum following FouriDown obtains the outstanding smooth response in both high and low frequencies.

4.4 Discussions

Bias Effects by Static Superposing. As shown in Figure 8, we compare different down-sampling methods with static superposing manner, and find they have various bias effects.

Frequency Aliasing Visualization. To delve deeper into the high-low frequency interactions in down-sampling, we examine the spectrum of images down-sampled by factors of 4x, 2x, and 1x. Following Theorem 1, some regions of spectrums are overlaid on the same frequency band, with smaller scales overlaying larger ones, as shown in Figure 9. This alignment of same bandwidth reveals a rectangular contour at the intersections, where high-frequencies not obeying the Nyquist theory fold into low frequencies during down-sampling, as pointed by the yellow arrow. This suggests that it is significant for down-sampling to modulate frequencies, otherwise it might degrade the original signal undesirably.

Other Discussions. Because of space constraints, for more discussions, including extensions to Theorem-2 and revisiting of previous anti-aliasing methods in the proposed FouriDown framework, could be referred to the supplementary material.

5 Limitations

In this work, we explore spatial down-sampling from a frequency-domain perspective and optimize the static weighting of previous down-sampling with a stride of 2 in the frequency domain. Our modeling of down-sampling is based on using uniformly distributed impulse sequences as the sampling function, hence exploring the characteristics of the sampling function in the frequency domain. However, for non-uniform down-sampling, where the sampling rate varies according to the content, our method might become limited. We hope to overcome this limitation in the future work by exploring the frequency domain response of non-uniform sampling functions.



Figure 8: The comparison of results by different down-sampling manner in $2x$ scale. In (b), which is the nearest down-sampling of (a), some unnatural stripes in the edge of windows and walls, called aliasing effects. To relieve the occurrence of aliasing, (c) and (d) employ the "ideal low-pass filter" and the Gaussian filter before down-sampling respectively. However, these manners usually lead to ringing effects or heavy high-frequency loss inevitably.

Config	LOL		FLOPs(G)	Para(M)
	PSNR	SSIM		
Bicubic	21.35	0.8497	13.764	7.84
Bilinear	21.26	0.8464	13.764	7.84
Pixle-shuffle	21.41	0.8552	13.954	8.11
Stride Conv	21.36	0.8534	13.954	8.11
Max pooling *	21.46	0.8584	13.753	7.84
Average pooling	21.34	0.8481	13.754	7.84
Gaussian	21.79	0.8612	16.102	8.54
LPF	20.74	0.8124	16.102	8.54
Ours	23.28	0.8708	13.827	7.87

Table 5: The effectiveness and efficiency comparison between our FouriDown and other down-sampling methods in low-light enhancement task.

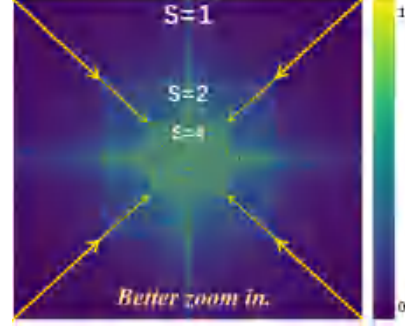


Figure 9: The spectrums of different-scale images placed under the same frequency coordinate system.

6 Conclusion

In our study, we revisit the spatial down-sampling techniques and anti-aliasing strategies from a Fourier domain perspective, recognizing their reliance on static high and low frequency superposing. As a result, we propose a novel approach (FouriDown) to learn a learnable frequency-context interplay among high and low frequencies during down-sampling. Moreover, this work is the first exploration of dynamic frequency interaction in down-sampling. The FouriDown is designed based on the signal sampling theory, so it is convenient to replace most of current down-sampling and anti-aliasing techniques. Extensive experiments demonstrate the performance improvements across a variety of vision tasks.

Ultimately, we believe that down-sampling is a crucial research direction in the future. It allows for network design at a lower resolution, significantly reducing the computational overhead and enabling light-weighting models.

Broader Impact

This work further exploits the potential of down-sampling in the Fourier domain and offers a new perspective that frequency band shuffling and superposing for future research of down-sampling. Down-sampling techniques can potentially make the future model development more efficient and effective, beneficial for various machine learning and AI applications. Nonetheless, the efficacy of our method could be a source of concern if not properly utilized, especially in terms of the safety of real-world applications. To alleviate such concerns, we plan to rigorously investigate the robustness and effectiveness of our approach across a more diverse spectrum of real-world scenarios.

Acknowledgments

This work was supported by the JKW Research Funds under Grant 20-163-14-LZ-001-004-01, and the Anhui Provincial Natural Science Foundation under Grant 2108085UD12. We acknowledge the support of GPU cluster built by MCC Lab of Information Science and Technology Institution, USTC.

References

- [1] Yongbing Zhang, Debin Zhao, Jian Zhang, Ruiqin Xiong, and Wen Gao. Interpolation-dependent image downsampling. *IEEE Transactions on Image Processing*, 20(11):3291–3296, 2011.
- [2] Ding-Xuan Zhou. Theory of deep convolutional neural networks: Downsampling. *Neural Networks*, 124:319–327, 2020.
- [3] Christian Bailer, Tewodros Habtegebrial, Didier Stricker, et al. Fast feature extraction with cnns with pooling layers. *arXiv preprint arXiv:1805.03096*, 2018.
- [4] Leif E Peterson. K-nearest neighbor. *Scholarpedia*, 4(2):1883, 2009.
- [5] Michael Lindenbaum, Shaul Markovitch, and Dmitry Rusakov. Selective sampling for nearest neighbor classifiers. *Machine learning*, 54:125–152, 2004.
- [6] Edward A Patrick and Frederic P Fischer III. A generalized k-nearest neighbor rule. *Information and Control*, 16(2):128–152, 1970.
- [7] Richard Zhang. Making convolutional networks shift-invariant again. *ArXiv*, abs/1904.11486, 2019.
- [8] Antônio H. Ribeiro and Thomas Schon. How convolutional neural networks deal with aliasing. *Proceedings of the IEEE International Conference on Acoustics, Speech and Signal Processing*, pages 2755–2759, 2021.
- [9] Cristina Nader Vasconcelos, H. Larochelle, Vincent Dumoulin, Nicolas Le Roux, and Ross Goroshin. An effective anti-aliasing approach for residual networks. *ArXiv*, abs/2011.10675, 2020.
- [10] Xueyan Zou, Fanyi Xiao, Zhiding Yu, and Yong Jae Lee. Delving deeper into anti-aliasing in convnets. *International Journal of Computer Vision*, 131:67–81, 2020.
- [11] Gaurav Parmar, Richard Zhang, and Jun-Yan Zhu. On aliased resizing and surprising subtleties in gan evaluation. *Proceedings of the IEEE/CVF Conference on Computer Vision and Pattern Recognition*, pages 11400–11410, 2022.
- [12] Shengju Qian, Hao-Chiang Shao, Yi Zhu, Mu Li, and Jiaya Jia. Blending anti-aliasing into vision transformer. In *Neural Information Processing Systems*, volume 34, pages 5416–5429, 2021.
- [13] Hagay Michaeli, Tomer Michaeli, and Daniel Soudry. Alias-free convnets: Fractional shift invariance via polynomial activations. *ArXiv*, abs/2303.08085, 2023.
- [14] Tsung-Yi Lin, Piotr Dollár, Ross B. Girshick, Kaiming He, Bharath Hariharan, and Serge J. Belongie. Feature pyramid networks for object detection. In *Proceedings of the IEEE Conference on Computer Vision and Pattern Recognition*, pages 936–944, 2016.
- [15] Naishan Zheng, Man Zhou, Yanmeng Dong, Xiangyu Rui, Jie Huang, Chongyi Li, and Feng Zhao. Empowering low-light image enhancer through customized learnable priors. In *Proceedings of the IEEE/CVF International Conference on Computer Vision (ICCV)*, pages 12559–12569, October 2023.
- [16] Xiang Chen, Jinshan Pan, Jiyang Lu, Zhentao Fan, and Hao Li. Hybrid cnn-transformer feature fusion for single image deraining. In *Proceedings of the AAAI Conference on Artificial Intelligence*, volume 37, pages 378–386, 2023.
- [17] Qi Zhu, Naishan Zheng, Jie Huang, Man Zhou, Jinghao Zhang, and Feng Zhao. Learning spatio-temporal sharpness map for video deblurring. *IEEE Transactions on Circuits and Systems for Video Technology*, 2023.
- [18] Qi Zhu, Man Zhou, Naishan Zheng, Chongyi Li, Jie Huang, and Feng Zhao. Exploring temporal frequency spectrum in deep video deblurring. In *Proceedings of the IEEE/CVF International Conference on Computer Vision*, pages 12428–12437, 2023.

- [19] Qi Zhu, Zeyu Xiao, Jie Huang, and Fengmei Zhao. Dast-net: Depth-aware spatio-temporal network for video deblurring. *Proceedings of the IEEE/CVF International Conference on Multimedia and Expo*, pages 1–6, 2022.
- [20] Naishan Zheng, Jie Huang, Qi Zhu, Man Zhou, Feng Zhao, and Zheng-Jun Zha. Enhancement by your aesthetic: An intelligible unsupervised personalized enhancer for low-light images. In *Proceedings of the 30th ACM International Conference on Multimedia*, pages 6521–6529, 2022.
- [21] Naishan Zheng, Jie Huang, Man Zhou, Zizheng Yang, Qi Zhu, and Feng Zhao. Learning semantic degradation-aware guidance for recognition-driven unsupervised low-light image enhancement. In *Proceedings of the AAAI Conference on Artificial Intelligence*, volume 37, pages 3678–3686, 2023.
- [22] Jie Huang, Feng Zhao, Man Zhou, Jie Xiao, Naishan Zheng, Kaiwen Zheng, and Zhiwei Xiong. Learning sample relationship for exposure correction. In *Proceedings of the IEEE/CVF Conference on Computer Vision and Pattern Recognition*, pages 9904–9913, June 2023.
- [23] Naishan Zheng, Jie Huang, Feng Zhao, Xueyang Fu, and Feng Wu. Unsupervised underexposed image enhancement via self-illuminated and perceptual guidance. *IEEE Transactions on Multimedia*, 2022.
- [24] Huikang Yu, Jie Huang, Yajing Liu, Qibang Zhu, Man Zhou, and Fengmei Zhao. Source-free domain adaptation for real-world image dehazing. *Proceedings of the 30th ACM International Conference on Multimedia*, 2022.
- [25] Wei Yu, Qi Zhu, Naishan Zheng, Jie Huang, Man Zhou, and Fengmei Zhao. Learning non-uniform-sampling for ultra-high-definition image enhancement. *Proceedings of the 31st ACM International Conference on Multimedia*, 2023.
- [26] Julia Grabinski, Steffen Jung, Janis Keuper, and Margret Keuper. Frequencylowcut pooling - plug & play against catastrophic overfitting. *ArXiv*, abs/2204.00491, 2022.
- [27] Julia Grabinski, Janis Keuper, and Margret Keuper. Fix your downsampling asap! be natively more robust via aliasing and spectral artifact free pooling. *ArXiv*, abs/2307.09804, 2023.
- [28] Wenzhe Shi, Jose Caballero, Ferenc Huszár, Johannes Totz, Andrew P. Aitken, Rob Bishop, Daniel Rueckert, and Zehan Wang. Real-time single image and video super-resolution using an efficient sub-pixel convolutional neural network. *2016 IEEE Conference on Computer Vision and Pattern Recognition (CVPR)*, pages 1874–1883, 2016.
- [29] Heewon Kim, Myungsub Choi, Bee Lim, and Kyoung Mu Lee. Task-aware image downscaling. In *European Conference on Computer Vision*, 2018.
- [30] Rachid Riad, Olivier Teboul, David Grangier, and Neil Zeghidour. Learning strides in convolutional neural networks. *ArXiv*, abs/2202.01653, 2022.
- [31] Chittesh Thavamani, Mengtian Li, Francesco Ferroni, and Deva Ramanan. Learning to zoom and unzoom. *2023 IEEE/CVF Conference on Computer Vision and Pattern Recognition (CVPR)*, pages 5086–5095, 2023.
- [32] Dmitrii Marin, Zijian He, Péter Vajda, Priyam Chatterjee, Sam S. Tsai, Fei Yang, and Yuri Boykov. Efficient segmentation: Learning downsampling near semantic boundaries. *2019 IEEE/CVF International Conference on Computer Vision (ICCV)*, pages 2131–2141, 2019.
- [33] Babak Ehteshami Bejnordi, Amirhossein Habibian, Fatih Murat Porikli, and Amir Ghodrati. Salisa: Saliency-based input sampling for efficient video object detection. *ArXiv*, abs/2204.02397, 2022.
- [34] Wenhan Yang Jiaying Liu Chen Wei, Wenjing Wang. Deep retinex decomposition for low-light enhancement. In *Proceedings of the British Machine Vision Conference*, 2018.
- [35] Jiang Hai, Zhu Xuan, Ren Yang, Yutong Hao, Fengzhu Zou, Fang Lin, and Songchen Han. R2rnet: Low-light image enhancement via real-low to real-normal network. *arXiv preprint arXiv:2106.14501*, 2021.

- [36] Chen Chen, Qifeng Chen, Jia Xu, and Vladlen Koltun. Learning to see in the dark. In *Proceedings of the IEEE Conference on Computer Vision and Pattern Recognition*, pages 3291–3300, 2018.
- [37] Wenhan Yang, Shiqi Wang, Yuming Fang, Yue Wang, and Jiaying Liu. From fidelity to perceptual quality: A semi-supervised approach for low-light image enhancement. In *Proceedings of the IEEE/CVF Conference on Computer Vision and Pattern Recognition*, pages 3063–3072, 2020.
- [38] Seungjun Nah, Tae Hyun Kim, and Kyoung Mu Lee. Deep multi-scale convolutional neural network for dynamic scene deblurring. In *Proceedings of the IEEE Conference on Computer Vision and Pattern Recognition*, pages 3883–3891, 2017.
- [39] Syed Waqas Zamir, Aditya Arora, Salman Khan, Munawar Hayat, Fahad Shahbaz Khan, Ming-Hsuan Yang, and Ling Shao. Multi-stage progressive image restoration. In *Proceedings of the IEEE/CVF Conference on Computer Vision and Pattern Recognition*, pages 14821–14831, 2021.
- [40] Shuochen Su, Mauricio Delbracio, Jue Wang, Guillermo Sapiro, Wolfgang Heidrich, and Oliver Wang. Deep video deblurring for hand-held cameras. *Proceedings of the IEEE Conference on Computer Vision and Pattern Recognition*, pages 237–246, 2017.
- [41] Ziyi Shen, Wenguan Wang, Xiankai Lu, Jianbing Shen, Haibin Ling, Tingfa Xu, and Ling Shao. Human-aware motion deblurring. In *IEEE International Conference on Computer Vision*, 2019.
- [42] Abdelrahman Abdelhamed, Stephen Lin, and Michael S Brown. A high-quality denoising dataset for smartphone cameras. In *Proceedings of the IEEE Conference on Computer Vision and Pattern Recognition*, pages 1692–1700, 2018.
- [43] Tobias Plotz and Stefan Roth. Benchmarking denoising algorithms with real photographs. In *Proceedings of the IEEE Conference on Computer Vision and Pattern Recognition*, pages 1586–1595, 2017.
- [44] Syed Waqas Zamir, Aditya Arora, Salman Hameed Khan, Munawar Hayat, Fahad Shahbaz Khan, Ming-Hsuan Yang, and Ling Shao. Learning enriched features for fast image restoration and enhancement. *IEEE Transactions on Pattern Analysis and Machine Intelligence*, 45:1934–1948, 2020.
- [45] Syed Waqas Zamir, Aditya Arora, Salman Khan, Munawar Hayat, Fahad Shahbaz Khan, and Ming-Hsuan Yang. Restormer: Efficient transformer for high-resolution image restoration. In *Proceedings of the IEEE/CVF Conference on Computer Vision and Pattern Recognition*, pages 5728–5739, 2022.
- [46] Hang Dong, Jinshan Pan, Lei Xiang, Zhe Hu, Xinyi Zhang, Fei Wang, and Ming-Hsuan Yang. Multi-scale boosted dehazing network with dense feature fusion. In *Proceedings of the IEEE/CVF Conference on Computer Vision and Pattern Recognition*, pages 2157–2167, 2020.
- [47] Xiaohong Liu, Yongrui Ma, Zhihao Shi, and Jun Chen. Griddehazenet: Attention-based multi-scale network for image dehazing. In *Proceedings of the IEEE/CVF international conference on computer vision*, pages 7314–7323, 2019.
- [48] Ruixing Wang, Qing Zhang, Chi-Wing Fu, Xiaoyong Shen, Wei-Shi Zheng, and Jiaya Jia. Underexposed photo enhancement using deep illumination estimation. In *Proceedings of the IEEE/CVF Conference on Computer Vision and Pattern Recognition*, pages 6849–6857, 2019.
- [49] Michaël Gharbi, Jiawen Chen, Jonathan T Barron, Samuel W Hasinoff, and Frédo Durand. Deep bilateral learning for real-time image enhancement. *ACM Transactions on Graphics*, 36:1 – 12, 2017.

Appendix A: Proofs of Theorem-1 and Theorem-2

Proof of Theorem-1: Shuffling and Superposing

To model the relationship between $f'(x)$ and $f(x)$, we stand on their derived continuous signal $g(x)$ by a specific sampling function. Note that the sampling functions $s_{\Delta T}(x)$ is defined as the sum of infinitely impulses units separated by ΔT intervals:

$$s(x, \Delta T) = \sum_{n=-\infty}^{\infty} \delta(x - n\Delta T). \quad (4)$$

Based on the Eq. (4), $f(x)$ and its down-sampling $f'(x)$ can be represented as

$$f(x) = g(x)s(x, \Delta T), \quad f'(x) = g(x)s(x, 2\Delta T). \quad (5)$$

According to the Fourier transform and convolution theorem, the aforementioned spatial sampling can be expressed in the Fourier domain as:

$$\begin{aligned} F(u) &= G(u) \star S(u, \Delta T) = \int_{-\infty}^{\infty} G(\tau) S(u - \tau, \Delta T) d\tau \\ &= \frac{1}{\Delta T} \sum_n \int_{-\infty}^{\infty} G(\tau) \delta\left(u - \tau - \frac{n}{\Delta T}\right) d\tau = \frac{1}{\Delta T} \sum_n G\left(u - \frac{n}{\Delta T}\right), \end{aligned} \quad (6)$$

where $G(u)$ and $S(u, \Delta T)$ are the Fourier transform of $g(x)$ and $s(x, \Delta T)$. From Eq. (6), it can be observed that the spatial sampling introduces the periodicity to the spectrum and the period is $\frac{1}{\Delta T}$.

Note that the sampling rates of $f(x)$ and $f'(x)$ are Ω_x and Ω'_x , the relationship between them can be written as

$$\Omega_x = \frac{1}{\Delta T}, \quad \Omega'_x = \frac{1}{2\Delta T} = \frac{1}{2}\Omega_x. \quad (7)$$

Before down-sampling, to focus on the following down-sampling operation, we assume that $f(x)$ adheres to the Nyquist sampling theorem, which implies that $u_{max} > \frac{1}{\Omega_x}$.

After down-sampling, according to Nyquist sampling theorem, a whole sub-frequency band is limited in $(0, \frac{\Omega_x}{2})$. Moreover, the resulted band is the superposition of two original bands, which denoted as

$$F'(u) = \mathbb{S}(F(u), F(\hat{u})), \quad (8)$$

where \hat{u} , u are the high frequency above the sampling rate and the low frequency below the sampling rate, respectively, and \mathbb{S} is superposition operator.

(1) In the positive sub-band, where $u \in (0, \frac{\Omega_x}{4})$, \hat{u} and \tilde{u} should satisfy

$$u \in (0, \frac{\Omega_x}{4}) \quad \text{and} \quad \hat{u} \in (\frac{\Omega_x}{4}, u_{max}). \quad (9)$$

According to the aliasing theorem, the high frequency \hat{u} is folded back to the low frequency:

$$\tilde{u} = \left| \hat{u} - \frac{(k+1)\Omega'_x}{2} \right|, \quad \frac{k\Omega'_x}{2} \leq \hat{u} \leq \frac{(k+2)\Omega'_x}{2} \quad (10)$$

where $k = 1, 3, 5 \dots$ and \tilde{u} is folded results by \hat{u} .

According to Eq. (9) and Eq. (10), we have

$$\tilde{u} = \frac{\Omega_x}{2} - \hat{u}, \quad \text{and} \quad \tilde{u} \in (\frac{\Omega_x}{2} - u_{max}, \frac{\Omega_x}{4}). \quad (11)$$

Then, according to Eq. (8) and Eq. (11), we attain

$$F'(u) = \begin{cases} F(u) & \text{if } u \in (0, \frac{\Omega_x}{2} - u_{max}), \\ \mathbb{S}(F(u), F(\frac{\Omega_x}{2} - u)) & \text{if } u \in (\frac{\Omega_x}{2} - u_{max}, \frac{\Omega_x}{4}). \end{cases} \quad (12)$$

According to Eq. (6), $F(u)$ is symmetric with respect to $u = \frac{\Omega_x}{2}$,

$$F(\frac{\Omega_x}{2} - u) = F(u + \frac{\Omega_x}{2}). \quad (13)$$

Further, $F(u + \frac{\Omega_x}{2}) = 0$ when $u \in (0, \frac{\Omega_x}{2} - u_{max})$. Upon Eq. (13), we can uniform Eq. (12) as

$$F'(u) = \mathbb{S}(F(u), F(u + \frac{\Omega_x}{2})) \quad \text{when } u \in (0, \frac{\Omega_x}{4}) \quad (14)$$

The visualization of the aforementioned proof process is depicted in Figure 2(a).

(2) In the negative sub-band, where $u \in (\frac{\Omega_x}{4}, \frac{\Omega_x}{2})$, different from (1), \hat{u} and \tilde{u} should satisfy

$$u \in (\frac{\Omega_x}{4}, \frac{\Omega_x}{2}) \quad \text{and} \quad \hat{u} \in (\frac{\Omega_x}{2} - u_{max}, \frac{\Omega_x}{4}). \quad (15)$$

Similarly, we can proof $F(u)$ in the negative sub-band as well.

$$F'(u) = \mathbb{S}(F(u), F(u + \frac{\Omega_x}{2})) \quad \text{when } u \in (\frac{\Omega_x}{4}, \frac{\Omega_x}{2}) \quad (16)$$

Combined with Eq. (14) and Eq. (16), we obtain

$$F'(u) = \mathbb{S}(F(u), F(u + \frac{\Omega_x}{2})), \quad \text{when } u \in (0, \frac{\Omega_x}{2}). \quad (17)$$

Proof of Theorem-2: Static Superposing.

According to Eq. (7) and Eq. (6), we can deduce that the amplitude of F' is half that of F .

Therefore, we can write $F'(u)$ in the x axis as,

$$F'(u) = \frac{1}{2}F(u) + \frac{1}{2}F(u + \frac{\Omega_x}{2}), \quad \text{when } u \in (0, \frac{\Omega_x}{2}). \quad (18)$$

Upon the dual principle, we can prove $F'(v)$ in the whole sub-band

$$F'(u, v) = F'(F'(u, y), v) = \frac{1}{4} \left(F(u, v) + F(u + \frac{\Omega_x}{2}, v) + F(u, v + \frac{\Omega_y}{2}) + F(u + \frac{\Omega_x}{2}, v + \frac{\Omega_y}{2}) \right), \quad (19)$$

where $u \in (0, \frac{\Omega_x}{2}), v \in (0, \frac{\Omega_y}{2})$.

Appendix B: Revisiting previous down-sampling manners in the FouriDown

In the main body, we introduce the FouriDown framework which can simultaneously adjust the stride of down-sampling and the characteristics of frequency interaction. Moreover, in the manuscript, we prove that the operator with a stride of 2 can be simplified to a fixed frequency weighting, *i.e.* averaging. However, this kind of weighting brings aliasing, hence the need for anti-aliasing methods such as ideal low-pass filters and Gaussian filters, which put focused weighting on frequencies. In this section, we revisit these anti-aliasing methods within the FouriDown framework and discover that their weighting methods remain fixed. In other words, within our framework, it's possible to realize the aforementioned anti-aliasing methods by simply changing specific parameters as shown in Figure 10 and 11.

Appendix C: Stride Extension of Theorem-1 and Theorem-2

In the manuscript, we propose FouriDown which primarily focuses on analyzing frequency interactions in the case of stride=2. In this section, we extend the Theorem-2 to arbitrary integer strides s , resulting in the following theorem. The proof for these theorems follow similar logic to that detailed in the main body, and is therefore omitted for brevity.

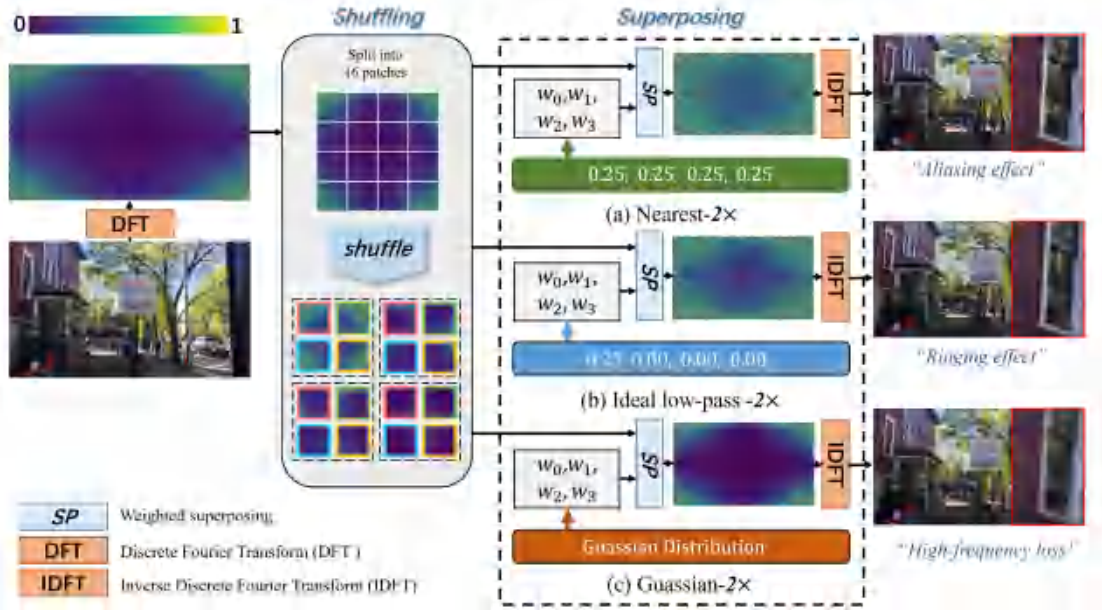


Figure 10: The achievements of different down-sampling manners in the FouriDown by simply changing specific parameters.

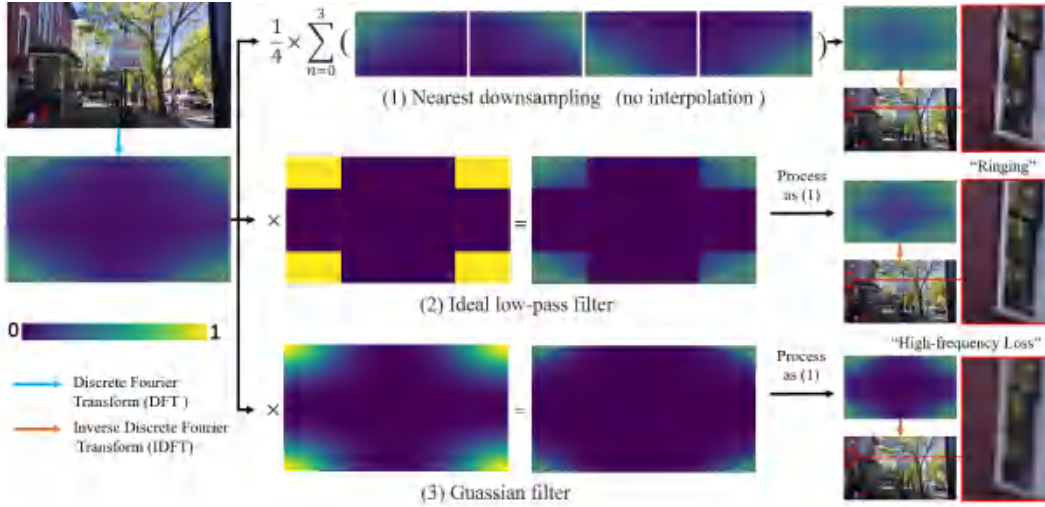


Figure 11: Revisiting different down-sampling methods from the perspective of spectrum.

Stride Extension of Theorem-1. In the condition of s strides, to illustrate with 1-dimensional signal, the high and low frequency superposition in the down-sampling can be formulated as

$$F'(u) = \mathbb{S}(F(u), F(u + \frac{k_i \Omega_x}{s})) \quad \text{when } u \in (0, \frac{\Omega_x}{2}), \quad (20)$$

where \mathbb{S} is a superposing operator and $k_i = 1, \dots, s-1$.

Stride Extension of Theorem-2. For an image, the spatial down-sampling operator with s strides can be equivalent to dividing the Fourier spectrum into $s \times s$ equal parts and superposing them averagely by $\frac{1}{s^2}$ factor

Given that Down_s is s -strided down-sampling operator and IDFT is inverse discrete Fourier transform, we have

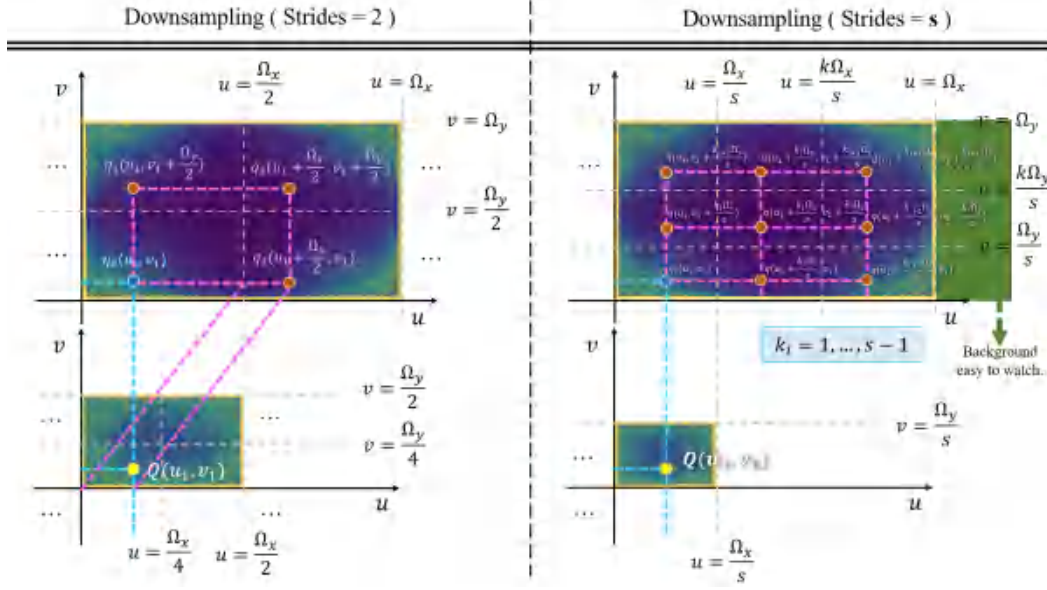


Figure 12: Illustration of theorem extension from $strides=2$ to $strides=s$. Due to visualization space limitation, s is taken as 3 in the figure. The background region has no meaning, just to show more clearly.

$$\text{Down}_s(f(x, y)) = \text{IDFT} \left(\frac{1}{s^2} \sum_{i=0}^{s-1} \sum_{j=0}^{s-1} F_{(i,j)}(u, v) \right). \quad (21)$$

Based on above extension, the down-sampling of 3 strides could be presented as in Figure 12.

Appendix D: More Qualitative comparison.

Due to the limited space, we only report the visual results of the low-light enhancement task in main manuscript. We report more visual results in the supplementary materials. As shown, integrating the FouriDown with the original baseline [36, 37, 48, 49, 39, 45, 44, 46, 47] achieves more visually pleasing results as shown in Figure 13 14 15 16 17.

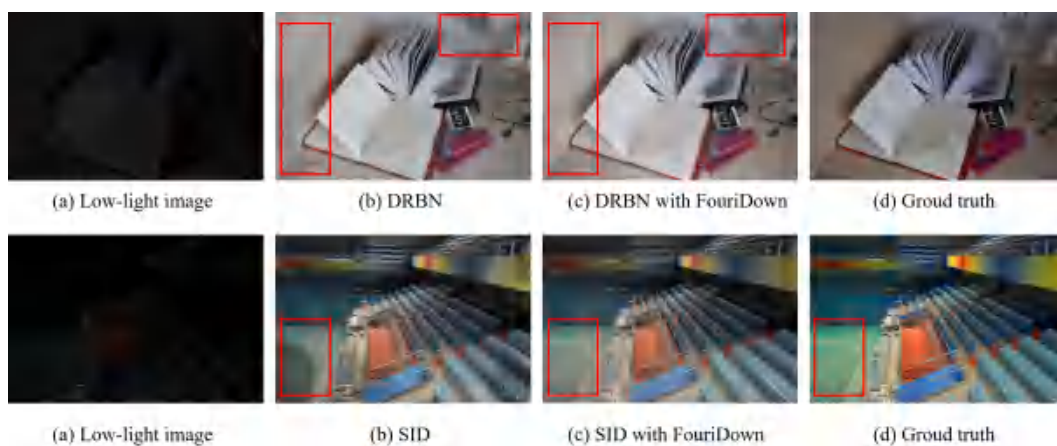


Figure 13: **Visual comparison on the low-light enhancement task.**

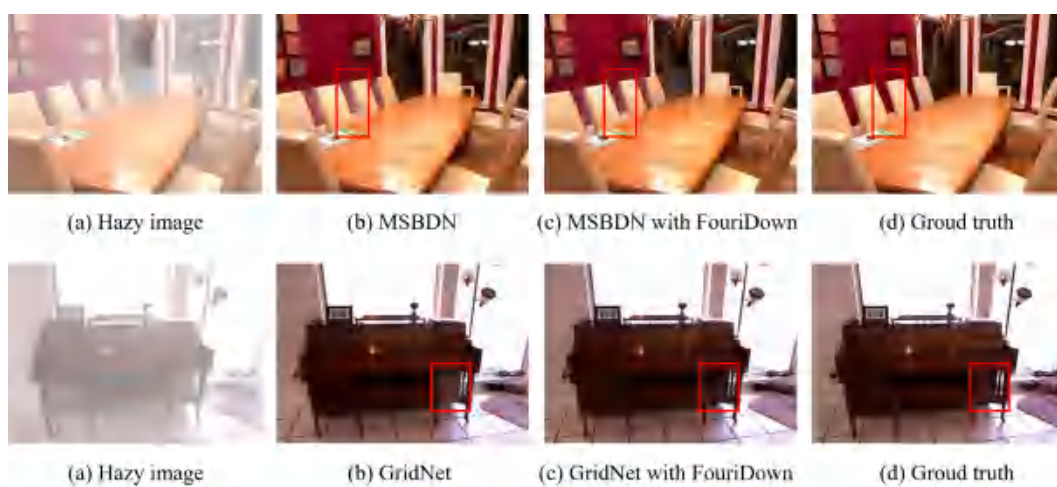


Figure 14: **Visual comparison on the dehazing task.**

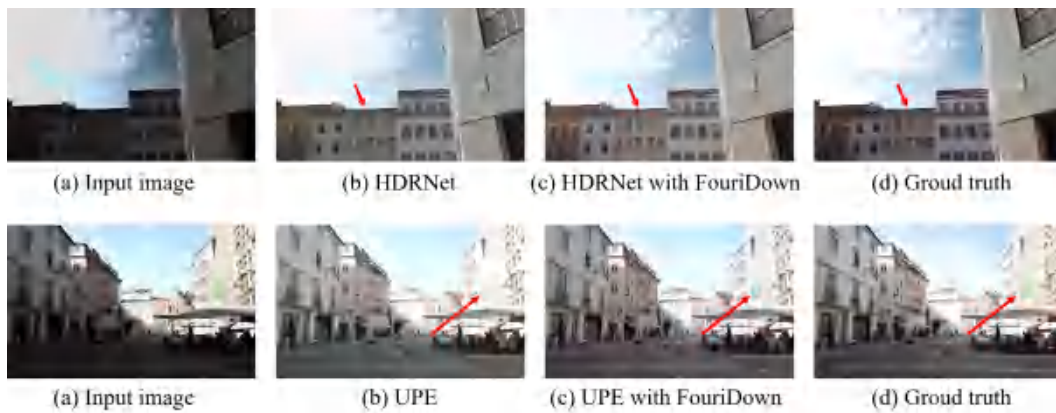


Figure 15: **Visual comparison on the UHD-enhancement task.**

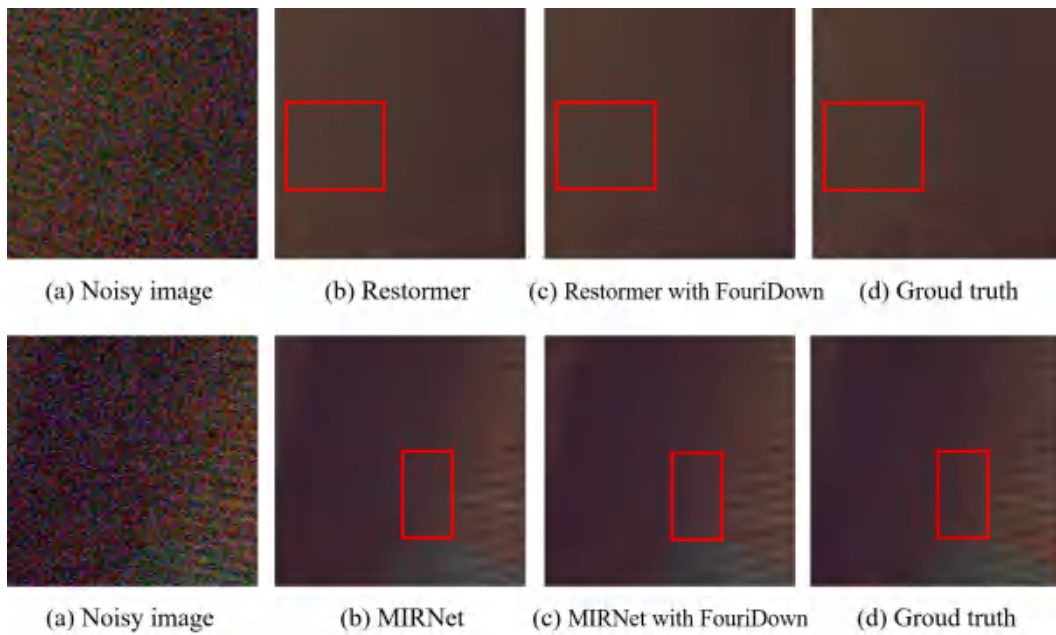


Figure 16: **Visual comparison on the denoising task.**

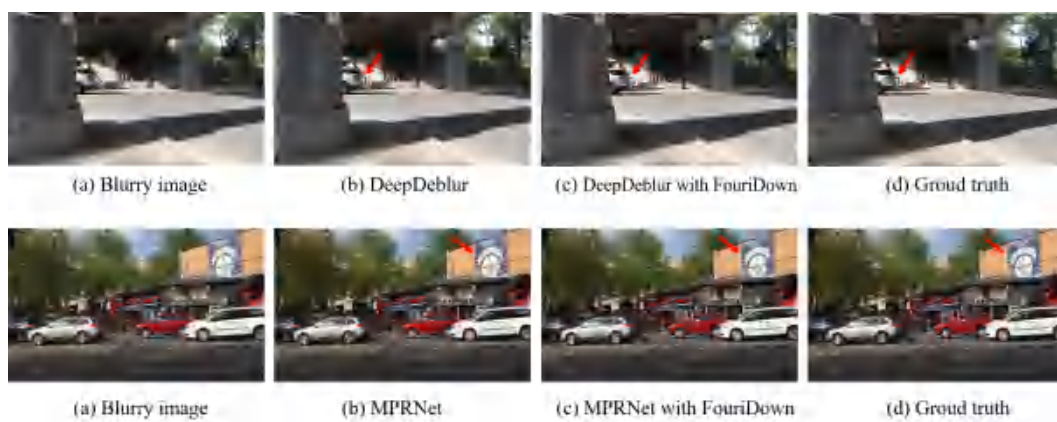


Figure 17: **Visual comparison on the deblurring task.**